OPERA HPC

OPEn HPC theRmomechanical tools for the development of eAtf fuels

Deliverable D3.2 – Results of the fuel reference state calculations

Version 1 – 09/07/2025

Funded by the European Union

Disclaimer

Document type	Deliverable
Document number	D3.2 version 1
Document title	Results of the fuel reference state calculations
Authors	G. Zullo, A.G. Segala, D. Pizzocri, L. Luzzi (POLIMI), L. Verma, I. Clifford (PSI), A. Tidikas, T. Kaliatka (LEI), P. Aragón, F. Feria (CIEMAT)
Release date	09/07/2025
Contributing partners	POLIMI, PSI, LEI, CIEMAT
Dissemination level	Public

Version	Short description	Main author	PMO	WP leader	Coordinator
1	First release	D. Pizzocri (POLIMI) Date 30/04/2025	S. de Grandis (Sintec) Date 27/05/2025	J. Heikinheimo (VTT) Date 17/06/2025	B. Michel (CEA) Date 09/07/2025

Abstract

This deliverable presents the results of fuel reference state calculations, with a focus on the chemical-physical material changes and the associated mechanical loading during transient scenarios, specifically Loss of Coolant Accident (LOCA) and Reactivity Initiated Accident (RIA). The calculations are performed using well-validated Fuel Performance Codes (FPCs), contributing to the understanding of fuel behaviour under these conditions. The task integrates the expertise and capabilities of multiple partners, ensuring the applicability and synergy of the different FPCs. The results aim to define the fuel reference initial states for transient scenarios and reference state variables during transient scenarios, providing valuable data for subsequent tasks and validation activities.

Table of contents

1 Introduction

The fuel reference state is a critical concept in the analysis of nuclear fuel behaviour, particularly during transient scenarios such as LOCA and RIA. The primary objective of Task 3.2 is to define the fuel reference state variables and initial conditions by calculating the chemical-physical changes in the fuel and the associated mechanical loading that occur during these transients. This task builds on the boundary conditions provided by Task 5.2, devoted to validation, and is closely linked to the objectives of Task 3.1. The collaboration between various partners, each using different FPCs, enables a comprehensive analysis by leveraging the unique capabilities and expertise of each code. The partner contributions in this task are as follows:

- PSI, as expert users of the fuel performance code Falcon from EPRI, runs base-irradiation and selected transient simulations for the chosen fuel design using Falcon.
- LEI provides RIA calculations using the TRANSURANUS code.
- POLIMI performs analyses with the TRANURANUS/SCIANTIX fuel performance suite, focusing on the definition of reference states for fission gas-related quantities.
- CIEMAT contributes to the simulation of LOCA and RIA scenarios with the U.S.NRC FAST code.

These contributions will ensure that the calculations and models used to define the fuel reference state are robust and comprehensive, supporting the objectives of Task 3.2 and enhancing the overall fuel performance analysis. The results of these calculations are essential for refining fuel performance models and enhancing the safety analysis of nuclear reactors.

2 Case description

2.1 IFA-650.10

The Halden Instrumented Fuel Assembly (IFA)-650.10 experiment is an integral in-pile single-rod test on fuel behaviour under simulated LOCA condition (Lavoil, 2010). The experiment used a segment cut from a standard Pressurized Water Reactor (PWR) fuel rod (Zircaloy-4 cladding and UO_2 fuel), previously irradiated in Gravelines 5 for five cycles.

Detailed information on the mother rod design, power history, and axial power distribution can be found in (Nishi & Lee, 2001).

The test rodlet was filled with a gas mixture of argon and helium and had a large plenum volume to maintain stable pressure conditions until cladding burst. The test was conducted at low constant fission power to achieve the desired conditions for cladding ballooning and high-temperature oxidation. The initiation of the blow-down phase involved opening the valves that allowed the water to flow from the bottom of the test rig to the dump tank. Consequently, the test rig pressure rapidly decreased, depleting most of its water content. The presence of stagnant superheated steam around the rodlet led to insufficient cooling, triggering the heat-up phase.

Further details on the test design and execution are reported in (Lavoil, 2010).

2.2 FK-1

The NSRR FK-1 experiment is an integral in-pile single-rod test focusing on fuel behaviour under simulated RIA conditions. The experiment used a rodlet refabricated from a segmented rod of the Boiling Water Reactor (BWR) 8x8BJ (STEP I) design, previously irradiated for five cycles (1984-1990) in the Fukushima Daiichi Nuclear Power Station Unit 3. The mother rod consisted of seven axial segments. The segment D7-5 (fifth segment from the bottom of the rod D7) was used for the FK-1 test.

Detailed information on the mother rod design and power history can be found in (Jernkvist, 2005; Sugiyama et al., 2004). Post-irradiation examinations (PIEs) performed on the D7-5 segment rod are described in (Sugiyama et al., 2004). Further details on the test design and execution are reported in (Sugiyama et al., 2004).

2.3 BEAVRS

The Benchmark for Evaluation And Validation of Reactor Simulations (BEAVRS) is a highly detailed PWR specification that can be used to validate high-fidelity core analysis methods. It was led by the MIT Computational Reactor Physics Group. The benchmark covers the first two cycles of the reactor operation and provides measured data including the operational power history, the critical boron concentration, the control rod worth, in-core fission-chamber-based detector signals, and isothermal temperature coefficients.

BEAVRS specification are available in (Horelik et al., 2018).

As part of Task 3.1, PSI carried out the postprocessing of the core follow simulations of the BEAVRS data done in an earlier study (Bykov et al., 2016) using CASMO-5 / SIMULATE-3 and CASMO-5 / SIMULATE-5. The postprocessing led to a clean set of boundary conditions for higher fidelity simulations. The data extracted included core loading map, operating boundary conditions, including core inlet temperature, core power, core flow and core outlet pressure, assembly power and burnup, and assembly boundary conditions including fuel temperature, moderator temperature and moderator density. For fuel behaviour simulations, pin power histories and boundary conditions for each fuel assembly were obtained by combining the cycle data for each

assembly with the pin-power reconstruction data. The time dependent linear heat generation rate and the axial power profile for the assembly containing peak burnup, as obtained from Task 3.1, were used as input to the Falcon analysis.

2.4 MT4

MT4 material test (Wilson et al., 1983) is one in a series of thermal-hydraulic and cladding mechanical deformation tests that were conducted in the National Research Universal (NRU) reactor at Chalk River National Laboratory in Canada. The major objectives of this program were to perform simulated LOCA experiments using full-length LWR fuel rods to study mechanical deformation, flow blockage, and coolability. In particular, the MT4 test aimed at providing sufficient time in the α-Zircaloy ballooning window of 1033 to 1200K to allow the test rods to rupture before reflood cooling was introduced, obtaining data for cladding ballooning and burst, and measuring the rod internal gas pressure during rod deformation.

3 Falcon simulations

At PSI, Falcon (Rashid et al., 2004) is the reference fuel behaviour analysis code. It has been well-validated for normal operating conditions as well as for accident scenarios. To obtain the fuel reference state, Falcon has been used to simulate the BEARVS benchmark rod for the base-irradiation and the MT4 material test for the LOCA scenario. The results obtained from Falcon provide a reference for corresponding simulations done with OFFBEAT, specifically as part of WP5 of the OperaHPC Project. In this section of the report, the two scenarios, for base-irradiation and LOCA, have been briefly described and the simulation results obtained using Falcon have been presented.

3.1 Base-irradiation simulation (BEAVRS)

For the Falcon analysis, a 2D axisymmetric geometry was adopted to simulate the full rod. The geometry was divided into 32 axial zones and 10 and 5 radial zones for the fuel and cladding, respectively. The material properties for the fuel and cladding were mostly adopted from MATPRO v11 (D. L. Hagrman & Reymann, 1979) available in Falcon. The radial power profile was calculated using the TUBRNP model (Lassmann et al., 1994). The creep models were based on the FCREEP subroutine of the MATPRO model (D. T. Hagrman et al., 1995) for the fuel and Limbäck and Andersson model (Limbäck & Andersson, 1996) for the zircaloy cladding. No fission gas release was assumed for this case. The power history and axial power profile was provided as input to Falcon, and the cladding outer surface temperature was fixed at 566 K. The simulation was carried out for both the cycles for a total simulation time of 920.22 days. Based on the simulation, the reference state for several parameters were obtained. Figure 1 shows some of the outputs from the Falcon simulation. From top left to bottom right, the figures represent fuel centreline and outer surface temperatures, cladding inner surface temperature, gap gas pressure, gap width, hoop stress on cladding inner surface and the fuel relocation strain. The simulation results from Falcon provide the reference state for the base-irradiation conditions. These results will be used to compare and refine the results obtained using OFFBEAT in WP5. Moreover, the 2-cycle base-irradiation condition will also be used in Task 3.3 to test the coupling and restart methodology adopted for an OFFBEAT 3D restart from a Falcon 2D input.

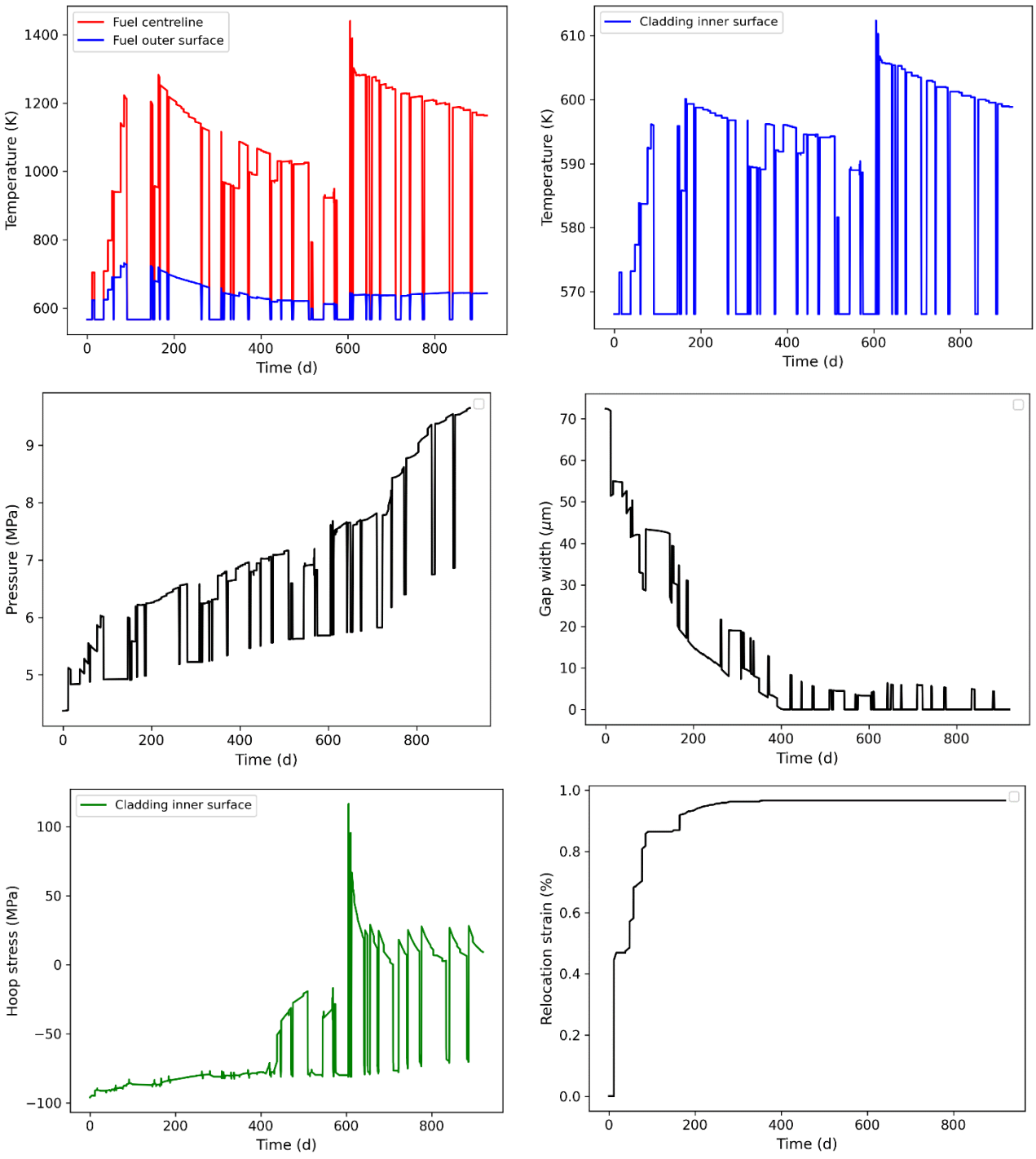

Figure 1: The reference state parameters as obtained using Falcon.

3.2 LOCA simulation (MT4)

A 2D axisymmetric geometry with 24 axial zones and 10 and 4 radial zones for the fuel and cladding, respectively, was used to simulate the full rod. The dimensions of the fuel and cladding were used based on the experimental data. The complete simulation comprised of a short heat up phase of 1.5 minutes reaching pre-transient conditions followed by a longer phase at temperature that lasted approximately 20 minutes before shutting off the steam flow. The fill gas pressure of 4.1 MPa was used to achieve the desired pre-transient gap gas pressure. The measured cladding temperature was provided as a time-dependent axial temperature profile to the cladding outer surface. For the creep modelling in the Zircaloy cladding, the Limbäck and Andersson model (Limbäck & Andersson, 1996) was used for standard temperature range and the equation of state from the MATPRO v11 was used for the high temperature regime (T>700 K). The assumed axial power profile and the pre-transient temperature profile provided as input to Falcon is shown in Figure 2.

The failure criteria for cladding rupture in Falcon is based on the Cumulative Damage Index (CDI), which calculates the damage based on the displacement of the rod with time. The cladding is considered ruptured when the CDI exceeds a threshold, provided as input. Once the threshold is reached, the gap internal pressure is equilibrated to the system pressure. Based on earlier validation studies on the Halden LOCA tests using Falcon (Khvostov et al., 2011), a threshold for CDI of 0.7 was considered for this simulation. The results obtained using Falcon were compared against measured experimental results for the gap gas pressure and the axial profilometry of the cladding ballooning, based on the hoop strain values. The comparison between Falcon and experiments for these two parameters are shown in Figure 3. The peak gas pressure reached in Falcon is higher than that in the experiments, however, the pressure at rupture is similar to the experimental observation. The axial profilometry based on the hoop strain at the cladding inner surface shows the ballooning area in close agreement to that observed in the experiment. The average hoop strain in the experiments was noted at ~72% with the maximum value reaching ~99%, whereas Falcon hoop strain for this simulation reached a maximum of 88.8%. The Falcon results for the different parameters are tabulated in Table 1.

The results for the MT4 test as obtained from Falcon are in close agreement with the experimental data. This Falcon analysis can now be used as a reference for the OFFBEAT validation of the MT4 LOCA test.

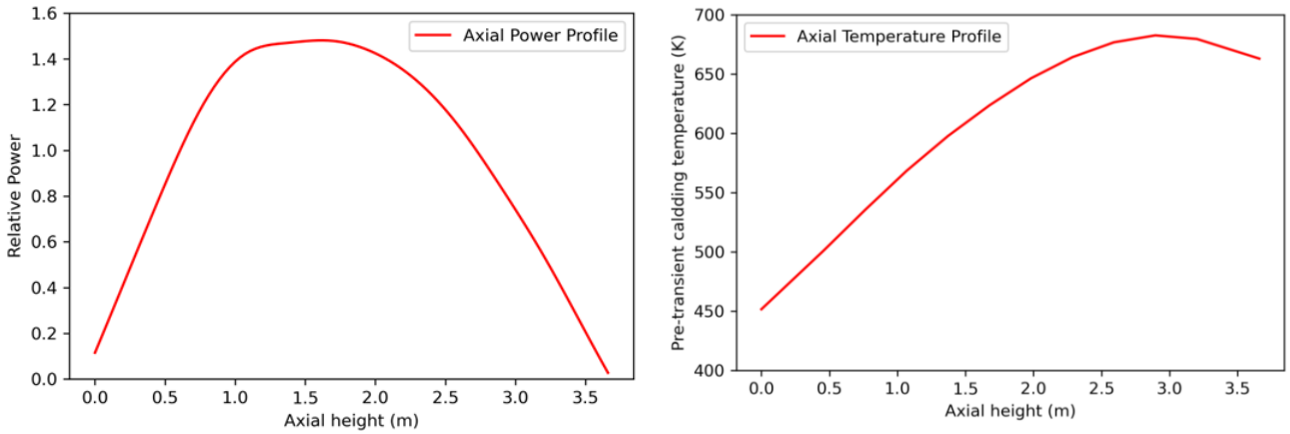

Figure 2: The axial power profile and pre transient temperature profile assumed for the simulations.

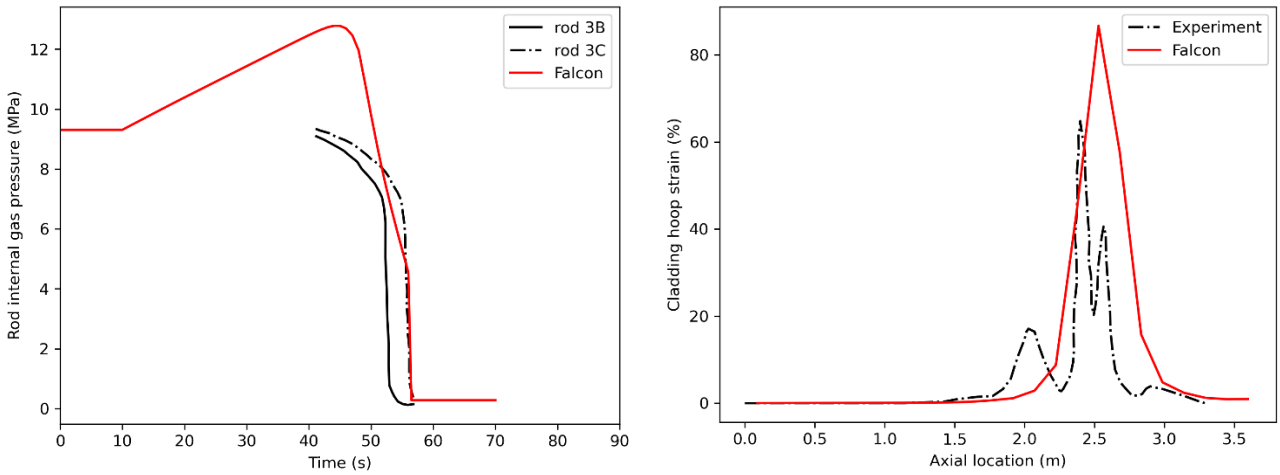

Figure 3: Results for the MT4 LOCA test using Falcon

Table 1: Experiment vs Falcon results for the gap gas pressure, hoop strain and rupture characteristics.

	Falcon
Rod pressure (MPa) Peak At rupture	 12.78 4.54
Hoop Strain (%)	86.83
Rupture time (s) (after steam off)	46.5
Rupture location (m)	2.53

4 TRANSURANUS simulations

4.1 TRANSURANUS RIA simulation (FK-1)

This section contains Lithuanian Energy Institute (LEI) contribution to the FK-1 RIA calculations. Calculations were performed with TRANSURANUS (v1m6j21) standalone code. Base irradiation history leads to a Burnup of 45 MWd/kgU in 5 years of operation. Additional 6 years were considered in the simulation, to represent the fuel storage until the RIA test. During the 6-year storage period, the fuel was assumed to be under zero linear heat rate (outer temperature 20 °C and outer pressure 0.1 MPa). As such, no significant changes were observed in fuel during the modelling period, aside from the natural decay of short-lived radionuclides. RIA test is initiated after restart sequence which is used to reset the filling gas pressure to 0.3 MPa, disable the relocation model and set the intergranular fission gas release model to the ramp conditions. The following TRANSURANUS settings were used:

- Intragranular fission gas diffusion is solved with the URGAS algorithm.
- Empirical intergranular fission gas release model is applied.
- Fuel densification is calculated with the TRANSURANUS LWR empirical model.
- STRECK model is used for the treatment of the fuel plasticity.
- Oxygen redistribution is not considered.
- Modified FRAPCON-3 relocation model (LWR conditions) is used.
- Subcooled boiling is considered.
- Fuel grain growth model from Ainscough and Olsen is considered.
- MATPRO outer corrosion model for BWR conditions is used.
- No pre-existing oxide layer was considered on the cladding.

The LHR was estimated from the illustrations of JAERI 2003 033 report. The 106 mm fuel rodlet was divided into 5 segments: from the bottom 5, 32, 32, 32, 5 mm. It is considered that the rodlet during transient receives uniform irradiation. There are 3 thermocouple measurements of the rod surface which is used as an input parameter in simulation to represent the fuel cladding temperature. This is achieved to prescribing thermocouple readings to the coolant and setting infinitely large heat transfer coefficient between coolant and cladding. It is important to note that thermocouples despite being named bottom, middle and top does not represent the fuel rod geometry. In this calculation, coolant data are described as such:

- Axial segment 1 (Thermocouple 1)
- Axial segment 2 (Thermocouple 2)
- Axial segment 3 (average of Thermocouple 2 and 3)
- Axial segment 4 (Thermocouple 3)
- Axial segment 5 (Thermocouple 3).

An interpolation was performed to fill the missing values for the TRANSURANUS simulation, as time intervals from thermocouple measurements poorly coincide with each other. The following figures contain graphs relevant for the analysis and result comparison. Additional data are provided in a separate file. All graphs, unless stated otherwise, give computational results for Axial segment 2 (Thermocouple 2). This segment represents the peak temperature of the cladding. However, the highest temperatures in the fuel centre (by a few degrees only) are given in the top and bottom axial segments.

When digitalizing transient, it was noted that the standard normal distribution doesn't fit too well as the transient peak in JAERI 2003 033 report lacks the mirror symmetry. A symmetrical description of the transient is adopted in default TRANSURANUS input files for FK RIA cases.

As seen in the Figure 8 difference for the fuel centreline temperature differs by 100-120°C. Away from the fuel centreline, the temperate difference decreases. For inner cladding surface temperatures at the time of the peak only differ by ~40 C and decreases towards the end of transient. Such results can have important consequences for the PCMI phenomena since it can influence gap closure and related mechanical properties.

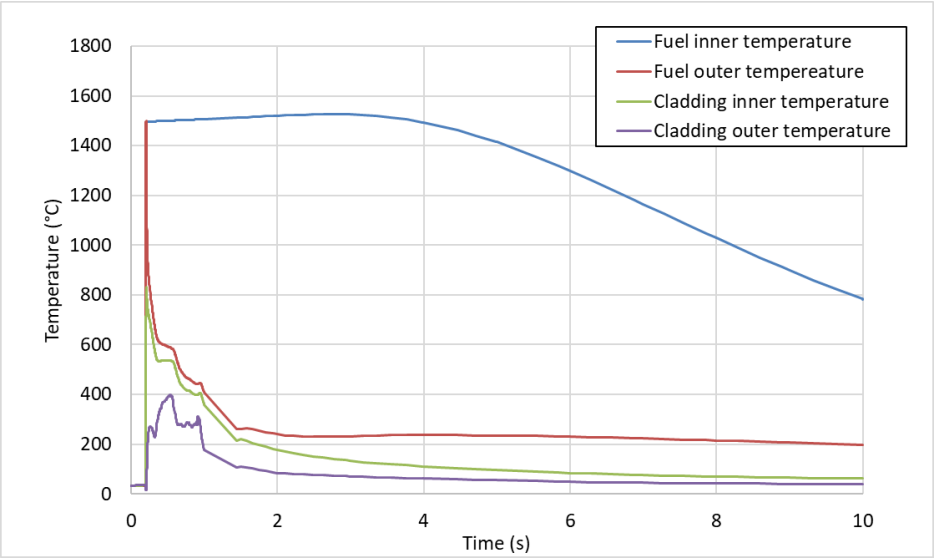

Figure 4. Fuel and cladding temperature profiles during the FK-1 transient simulations using TRANSURANUS. The plot shows the evolution over time of the inner and outer fuel temperatures, as well as the inner and outer cladding temperatures at the axial node corresponding to peak power. The sharp initial temperature rise corresponds to the RIA pulse, followed by a rapid drop due to heat transfer to the coolant and fuel-cladding gap reopening.

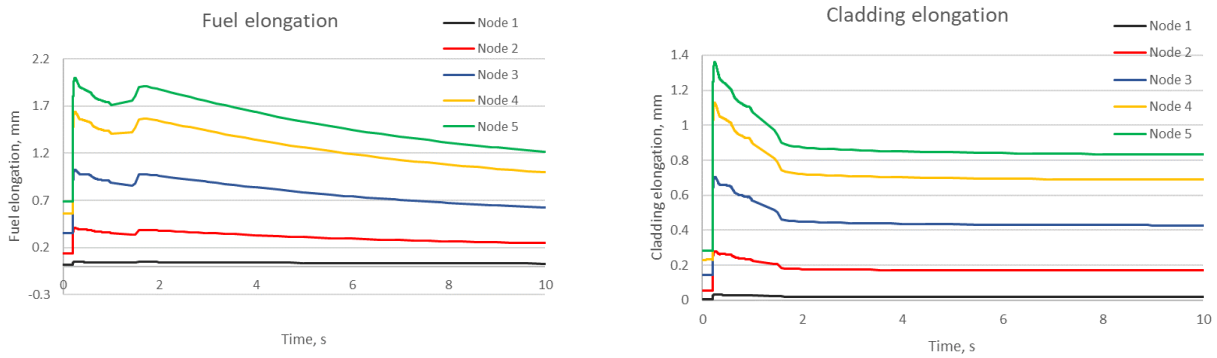

Figure 5. FK-1 simulations: fuel elongation (left) and cladding elongation (right) over time at five axial nodes. Results from TRANSURANUS show the mechanical response during the RIA pulse, with peak elongation observed near the axial location of maximum power. The trends reflect thermal expansion and transient gas pressure effects.

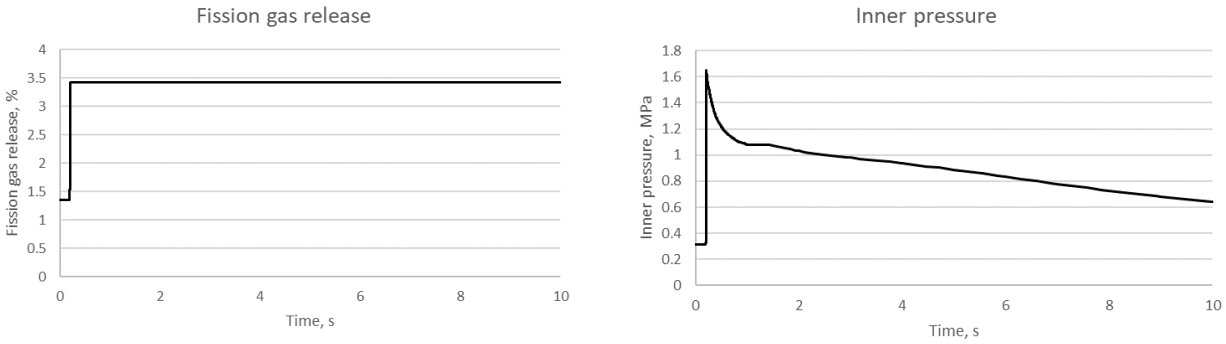

Figure 6. FK-1 simulations: fission gas release (left) and rod internal pressure (right) over time. Results from TRANSURANUS show a rapid gas release at the start of the transient, followed by a gradual decrease in internal pressure due to fuel cooling.

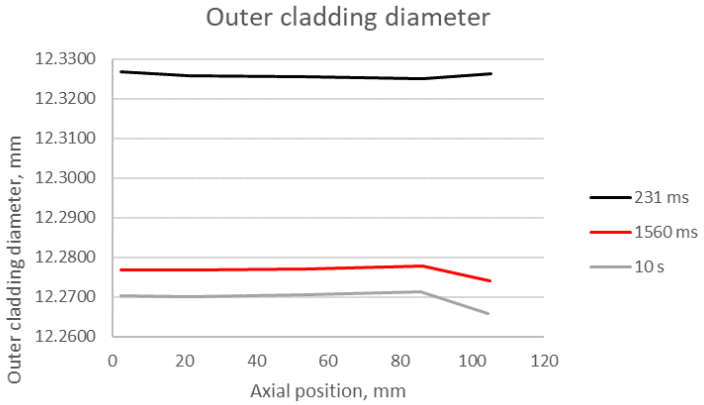

Figure 7. Cladding outer diameter profiles from FK-1 simulations at three time steps: 231 ms (peak temperature), 1560 ms (end of transient heat flux), and 10 s (end of calculation). The plot shows the evolution of cladding deformation along the axial position, highlighting the localized swelling due to thermal and mechanical loading during the RIA pulse.

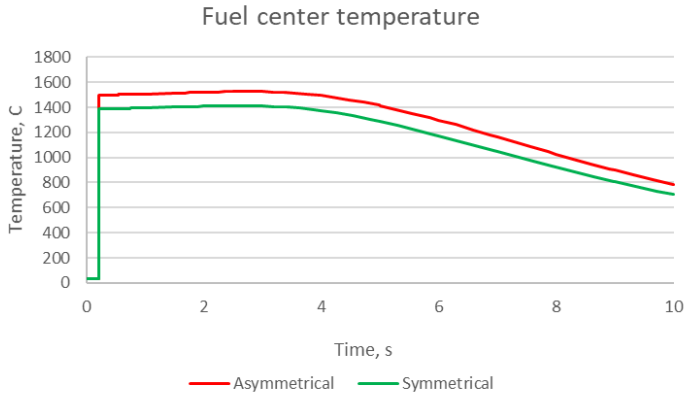

Figure 8. Comparison of fuel centerline temperature for FK-1 simulations using asymmetrical (red) and symmetrical (green) power pulses. The asymmetrical profile leads to slightly higher peak temperatures due to a longer tail in the power distribution.

4.2 TRANSURANUS/SCIANTIX RIA simulation (FK-1)

POLIMI simulated the FK1 RIA test with TRANSURANUS coupled with SCIANTIX. The figures of merit on which POLIMI focused are temperatures of fuel and cladding, transient FGR, gap width evolution and those for which experimental data are available, which are the fuel stack and cladding elongation and the internal pressure of the fuel rod. For what concern the calculated fuel and cladding temperatures, they are well aligned with the TRANSURANUS simulations, and the very slight differences are due to the different approaches to the fission gas release during the pulse test. The results are shown in Figure 9.

However, it should be noted that the measured cladding surface temperature reached about 350-400 °C but from post-irradiation examinations (Vickers hardness) a higher cladding temperature was envisaged due to locally occurring departure to nucleate boiling (DNB), which could be correlated with a plastic deformation of the cladding. During FK-1 pulse tests, cladding temperature was estimated to have reached about 600 °C. The FGR shown in Figure 10 highlights a burst release process, as expected under RIA condition. Unlike TRANSURANUS, TRANSURANUS coupled with SCIANTIX predicts an increasing gas release over time instead of a constant one since the simulation implements a detailed physical model based on diffusion, trapping, and resolution instead of semi-empirical models. The experimental transient FGR is around 8.2 %, that is over-estimated by calculations (Figure 10), likely due to an over-estimation of the fission gas accumulated in grain-boundary bubbles during the base irradiation. Post-irradiation examinations proved a uniform release especially from the central region (Sugiyama et al. 2004), and both temperature and FGR results are consistent with a release preferably occurring in the central region of the pellet up to the mid-radius. Hence, an accurate evaluation of the pre-pulse fission gas inventory is essential to properly quantify the fractions retained in the matrix, accumulated in grain-boundary bubbles, released through athermal mechanisms, and released via percolation-driven processes.

As expected, a sudden increase in temperatures and an instantaneous release of fission gases result in an immediate increase in the internal pressure in the gap, followed by a decreasing trend in accordance with the greater impact of the temperature drop just after the pulse compared to the growing FGR over time.
In this case as well, experimental data were available, shown in Figure 11. However, at the moment of the power pulse, a negative peak was recorded in every test, likely due to the generation of electrical charge in the pressure sensor induced by pulsed irradiation. Consequently, there is reason to believe that the values measured immediately after the power pulse are distorted and do not represent the actual gas pressure.

The rapid increase in the temperature of the fuel leads to its expansion and as mentioned earlier, to an increase in the internal pressure of the gap, also due to the release of fission gases. This is reflected in the evolution of the gap width, which closes in coincidence with the pulse, as shown in Figure 11.

For the elongations of the fuel and cladding (Figure 12), the results are fairly in line with the measured values but still underestimated, although the cladding elongation peak occurs somewhat prematurely, whereas for fuel it happens later. This behaviour, confirmed in (Suzuki 2010), could be possibly due to the lack of pre-conditioning in the experimental procedure (NEA 2010). Moreover, in the time interval 0.2-1 s, where this pronounced deviation is seen, cladding temperatures reach their maximum. It is therefore noted that the code deviates from the experimental response in coincidence with suspected DNB. In conclusion, the underestimation of both axial elongations for fuel and cladding highlights the need for an improved modelling of this phenomenon to better capture the fuel and cladding deformation mechanisms.

Figure 13 shows a simulation performed with TRANSURANUS integrated with SCIANTIX to calculate fuel deformation due to gaseous swelling. The difference in deformation before and after the pulse test can be observed; in particular, after the pulse, there is a general increase in deformation, which is more pronounced in the central and inner regions of the fuel. This could indicate that during the pulse, gas release causes greater expansion in these areas as the temperature reaches its peak in this region. As expected, the two

curves follow a similar trend, with higher swelling values after the pulse, indicating that the mechanism accelerated due to the sudden increase in temperature and intragranular gas pressure. Toward the periphery of the fuel, the two curves tend to converge, highlighting that the effect of the transient is less pronounced in the outer regions of the fuel.

Table 2. SCIANTIX settings used in TRANSURANUS-SCIANTIX simulations.

Fuel grain growth model	Ainscough et al. (1973)
Intra-granular fission gas diffusivity	Turnbull J.A. et al. (1988)
Intra-granular diffusion solver	Pastore et al. (2018)
Intragranular bubble evolution	Pizzocri et al. (2018)
Re-solution rate	Turnbull J.A. et al. (1971)
Trapping rate	Ham F.S. (1958)
Nucleation rate	Olander D.R. et al. (2006)
Grain-boundary vacancy diffusivity	White et al. (2004)
Grain-boundary bubbles behaviour	Pastore et al. (2013)
Grain-boundary microcracking	Barani et al. (2017)

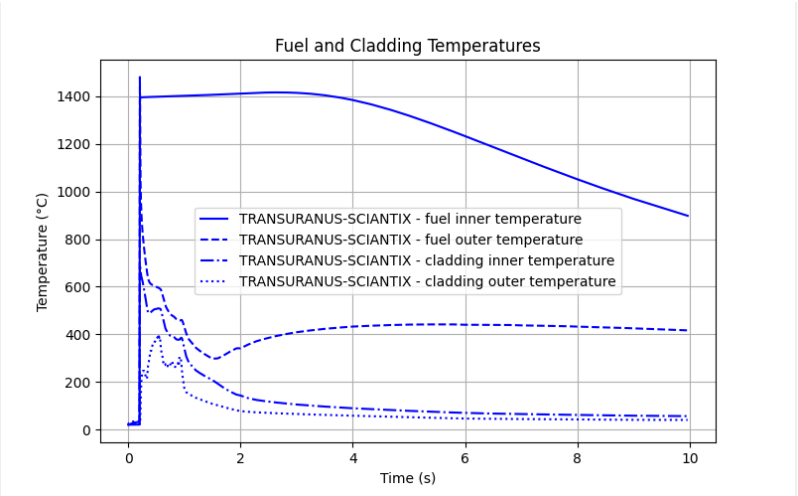

Figure 9: TRANSURANUS-SCIANTIX, FK1 fuel and cladding temperatures.

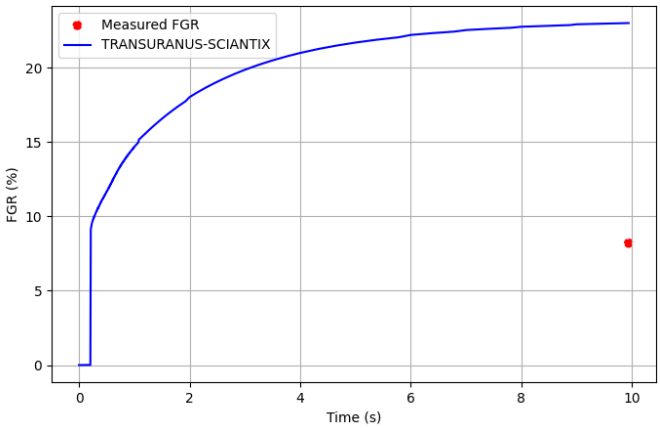

Figure 10: Transient FGR during pulse test.

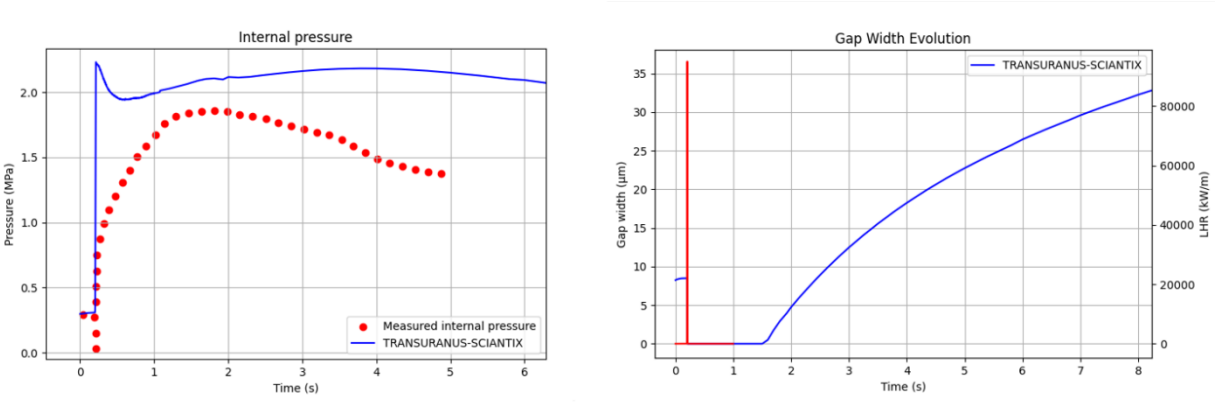

Figure 11: Rod internal pressure (left) and gap width evolution during pulse test (Jernkvist, 2005).

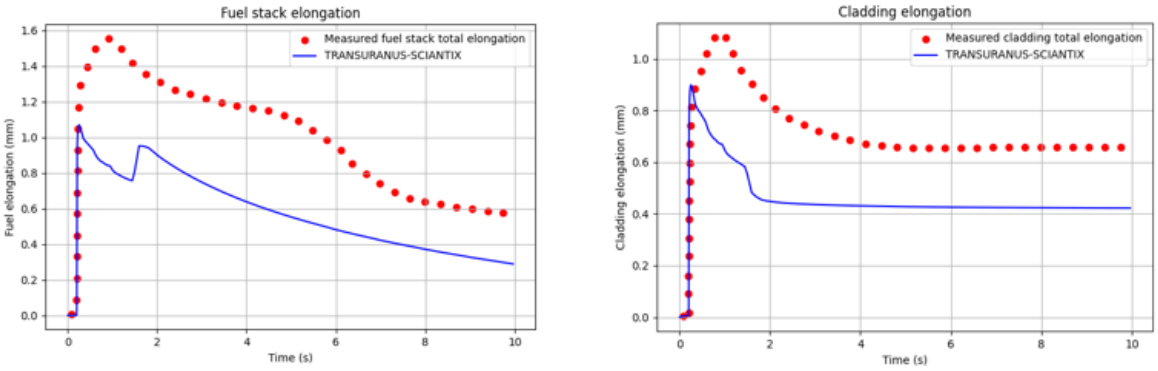

Figure 12: Fuel and cladding elongation (Jernkvist, 2005)..

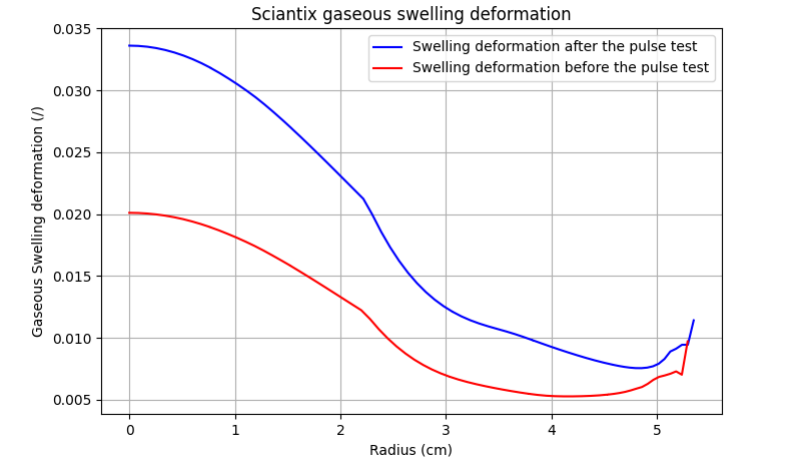

Figure 13: Sciantix gaseous swelling deformation pre and post pulse test.

5 FAST simulations

5.1 LOCA simulation (IFA-650.10)

Model settings

The simulation has been done by CIEMAT with the U.S. Nuclear Regulatory Commission code FAST-1.2.1 (Geelhood et al., 2022). Developed by Pacific Northwest National Laboratory (PNNL). FAST calculates the steady-state and transient thermo-mechanical response of a single fuel rod under normal operating conditions, anticipated operational occurrences, design basis accidents, and dry storage conditions, up to a rod average burnup of 62 MWd/kgU. The code relies on an updated version of the MATPRO material properties library. FAST is an evolution of the former PNNL codes FRAPCON and FRAPTRAN, which were developed to calculate the steady-state and transient response of light water reactor (LWR) fuel rods, respectively. In the simulation, the default models and options in FAST are applied unless otherwise specified. Below is a brief overview of the key models, options, assumptions, and boundary conditions used in the simulation.

The coolant inlet temperature, coolant pressure, and coolant mass flux as a function of time are fed into FAST. Their values correspond to the input data mentioned in the section 2.1, except for the coolant inlet temperature and pressure at end-of-cycle time steps, which are set to 25°C and 0.1 MPa, respectively. During the LOCA transient, the evolution of the cladding surface temperature and the coolant (test rig) pressure are specified. Data on the evolution of the test rig pressure have been digitized from the Halden report (Lavoil, 2010). The cladding surface temperature evolution at 26 axial elevations along the entire length of the rodlet was calculated by the Nuclear Safety Institute (IBRAE) using the T/H code SOCRAT/V3, within the FUMAC project. Since the top 8 axial nodes are positioned above the fuel stack column, their cladding surface temperatures could not be directly specified in FAST. Instead, the average cladding surface temperature from these top nodes has been fed into the code as the plenum gas temperature, assuming a minimal impact from the thermal resistance introduced by the cladding wall and the presence of the hold-down spring. This was achieved by defining an external plenum volume, currently the only method for specifying the plenum temperature as a function of time in FAST. The external plenum has a constant volume of 17 cm^3 that remains unchanged over time. Figure 19 illustrates the test rig pressure, the range of cladding surface temperatures along the active length of the rodlet, and the plenum gas temperature evolution. After the blowdown (occurring at 100 s), both the cladding surface and plenum temperatures gradually decrease as the test rig depressurizes and is emptied of water. The rise in plenum temperature is delayed compared to the cladding heat-up due to the slower axial propagation of heat through the gas.

The plenum temperature model is specified by the user. The default model in FAST for calculating the mechanical response of the fuel rod is the FRACAS-I model (Bohn, 1977). This model performs a small-strain analysis to evaluate stresses, strains, and displacements along the active length of the rod. It considers the effects of pellet thermal expansion, swelling, densification, and relocation; cladding thermal expansion, irradiation growth, creep, and plasticity; and fission gas and external coolant pressures. FRACAS-I assumes that the cladding retains its cylindrical shape during deformation and does not account for stress-induced deformation of the pellet. Due to this latter approximation, it is referred to as the rigid pellet model. After the cladding deformation has been calculated by FRACAS-I, a check is made to determine whether the cladding ballooning model should be activated. This check involves comparing the cladding effective plastic strain with the cladding instability strain given by MATPRO. If the effective plastic strain exceeds the instability strain, the BALON2 model is used to calculate the localized, non-uniform straining of the cladding. For details on the BALON2 model, refer to (D. L. Hagrman, 1981).

FAST includes two distinct cladding failure models. The low-temperature model is mainly applicable to reactivity-initiated accidents (RIAs), where pellet-cladding mechanical interaction (PCMI) drives cladding deformation while its temperature remains relatively low (< 700 K). This model is formulated as a strain limit that depends on the average temperature and hydrogen concentration in the cladding (Geelhood et al., 2008). The high-temperature model applies to LOCA events and the post-departure from nuclear boiling (post-DNB) phase of certain RIAs, where deformation results from internal gas overpressure combined with a relatively high cladding temperature (> 940 K). This model relies on empirical stress and strain limits to predict cladding failure. It is important to note that in the high-temperature failure model, the strain limit depends solely on temperature and is activated above 940 K, while the stress limit is activated only with the BALON2 model. Therefore, there are no defined strain limits between 700 K and 940 K.

The FRAPFGR model is used to initialize the transient release model in FRAPTRAN (now incorporated into FAST). If the (default) Forsberg-Massih model is selected instead of FRAPFGR, the transient release of fission gas will not be calculated. The transient release model is a burst (not diffusion) release model developed to predict the measured data from RIA tests in CABRI and NSRR. The Cathcart-Pawel (default) model is activated when the cladding temperature exceeds 1073 K (800°C).

Refabrication: The refabrication option is activated at the final time step of the base irradiation simulation, which corresponds to a zero-power cold state (i.e., 0 kW/m, 25°C, and 0.1 MPa).

Variable axial node length: The variable axial nodalization option is activated to precisely define the position of the test segment within the mother rod (905-1346 mm) from the start of the base irradiation. The mother rod is divided into 28 variable-length axial nodes, while the test rodlet nodalization comprises 20 nodes evenly spaced along its active length.

Results and discussion

The target output variables are the evolution of the rodlet internal gas pressure, cladding hoop stress, cladding permanent hoop strain evolution, the cladding burst time and the post-test cladding outer diameter profilometry. The simulation results from FRAPTRAN-2.0 are also included to verify the FAST predictions. Figure 15 shows the predictions of the rod internal gas pressure from the base case simulation, where the FAST input file strictly follows the test specifications and modelling options outlined above. The main observation is that, although the predictions from FRAPTRAN and FAST appear to evolve in parallel during most of the LOCA transient, with differences arising close to cladding burst, their initial internal gas pressures differ by roughly 3 MPa. The FAST simulation starts at 4 MPa, corresponding to the cold-state initial fill gas pressure specified for the test rodlet. This value was also specified in the FRAPTRAN simulation via the FRAPCON restart file[1]. However, unlike FAST, FRAPTRAN correctly calculates the hot-state initial gas pressure, as indicated by the good agreement with the experimental value. Figure 15 suggests that FAST incorrectly uses the user-specified initial fill gas pressure of the rodlet as the hot-state value. It should be noted that when building the FAST input file via the input generator, the temperature associated with the fill gas pressure at the time of refabrication cannot be specified. Consequently, it must be defined internally within the source code at an arbitrary (high) value.

Considering the above observation, the next step is to fine-tune the refabrication fill gas pressure to match the experimental value at the onset of blowdown (t = 100 s). The result, labelled as FAST (refab), is shown in Figure 15. The agreement between FRAPTRAN and the new FAST prediction is consistent until around 260 s into the simulation. At this point, the rodlet internal gas pressure calculated by FAST starts decreasing, while the FRAPTRAN prediction continues to rise until 280 s. In both simulations, the reduction of internal pressure

[1] In the FRAPCON restart file, the number of gas moles is specified. This value is calculated using the ideal gas law, assuming a gas volume of 17 cm^3 and a temperature of 25 °C.

stems from the onset of cladding permanent deformation, which triggers a significant increase in the free volume of the rodlet that eventually dominates over the effect of the rising temperature. These results suggest that the onset of permanent deformation occurs earlier in FAST. Moreover, the time elapsed between the onset of cladding permanent deformation and the transition from FRACAS-I to BALON2 - indicated by the discontinuity when reaching the instability strain - is much shorter in the FAST simulation but leads to a significantly lower increase in free volume. This raises the questions of whether the high strain rate cladding deformation model (CSTRNI) and/or the instability strain (set at 5% in FRAPTRAN) have been modified. However, the latter possibility has been ruled out, as the predicted cladding permanent hoop strain evolution shows a clear discontinuity precisely at 5%. It is possible, though this remains a hypothesis, that the low strain rate cladding deformation model (CSTRAN), which is only used during closed-gap regimes in FRAPTRAN, is also being applied during open-gap regimes in FAST, instead of CSTRNI. Regarding the cladding burst time, evidenced by the sharp drop in the rodlet internal gas pressure to meet the test rig pressure, FAST predicts failure 20 s earlier than FRAPTRAN, resulting in a 52 s underestimation relative to the experimental value.

Figure 16 illustrates the FAST prediction without activating the option to define an external plenum volume to specify its gas temperature evolution. Initially, there is good agreement as the test rig depressurizes and empties of water. However, around 75 s after the blowdown, the rodlet becomes completely surrounded by superheated steam, causing the cladding to heat up. From this point, using the default plenum temperature model in FAST leads to a significant overestimation of the rodlet internal gas pressure. This results in a larger underestimation of the burst time compared to the previous FAST simulations. Figure 16 highlights the importance of activating the user-specified external plenum temperature option in FAST when simulating the IFA-650.10 test. In the FRAPTRAN simulation, the pitch distance during the LOCA transient was set to match the inner diameter of the test rig pressure flask (34 mm), considering the absence of adjacent rods. In FAST, the same pitch must be used for both the base irradiation and the transient, as they share the same input file. Consequently, the approach adopted with FRAPCON/FRAPTRAN could not be applied, and a constant pitch of 12.6 mm has been used throughout the entire simulation. To assess the effect of imposing this pitch on the IFA-650.10 (single-rod) test, an additional FAST simulation was conducted with the pitch set to 34 mm, also during the base irradiation. However, no impact was observed on the rodlet internal gas pressure evolution during the LOCA transient.

The evolution of the cladding hoop stress and permanent hoop strain at the ballooning node, along with the post-test cladding outer diameter profilometry, are presented below only for the best-estimate FAST simulation, previously labelled as FAST (refab). Several observations can be made, some of which have been already discussed in relation to the rod internal gas pressure evolution: Figure 17 shows that cladding hoop stress calculations in FRAPTRAN and FAST are consistent until differences arise in their predictions of cladding permanent hoop strain around 260 s into the transient (see Figure 18). The maximum cladding hoop stress is 536 MPa for FRAPTRAN and 133 MPa for FAST. As depicted in Figure 18, the onset of cladding permanent deformation occurs earlier in FAST, and the time between this onset and the transition from FRACAS to BALON2 (which occurs at the 5% instability strain) is much shorter. Additionally, a discontinuity in cladding permanent hoop strain is observed in the FRAPTRAN simulation at the transition. In contrast, although the transition in FAST is not smooth, no discontinuities are evident. The maximum cladding permanent hoop strain is 66% for FRAPTRAN and 86% for FAST. Regarding the post-test cladding outer diameter profilometry shown in Figure 19, FAST predicts slightly less deformation for non-ballooning nodes, while the axial elevation of the ballooning node is closer to the experimental result compared to FRAPTRAN. However, the overprediction of cladding deformation at the ballooning node remains significant. In both simulations, the value diverges so markedly from the others that it had to be omitted to prevent distortion of the figure.

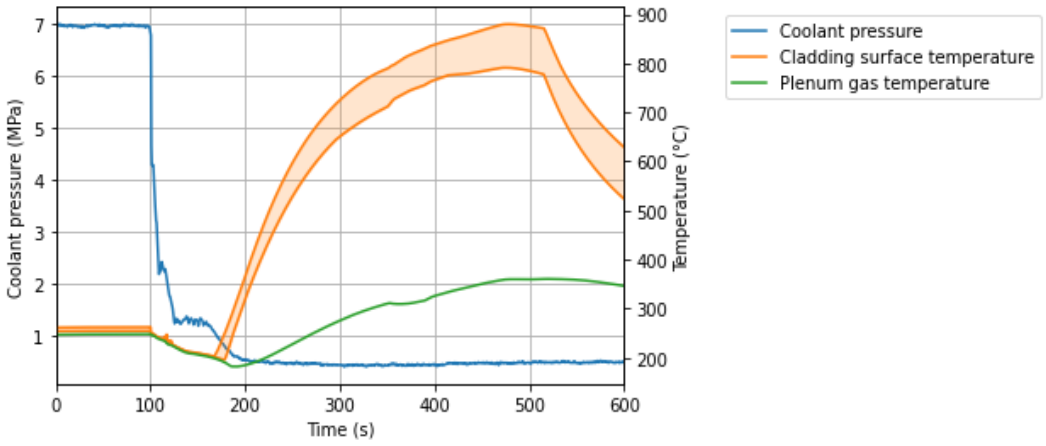

Figure 14. Time-dependent boundary conditions for IFA-650.10 test.

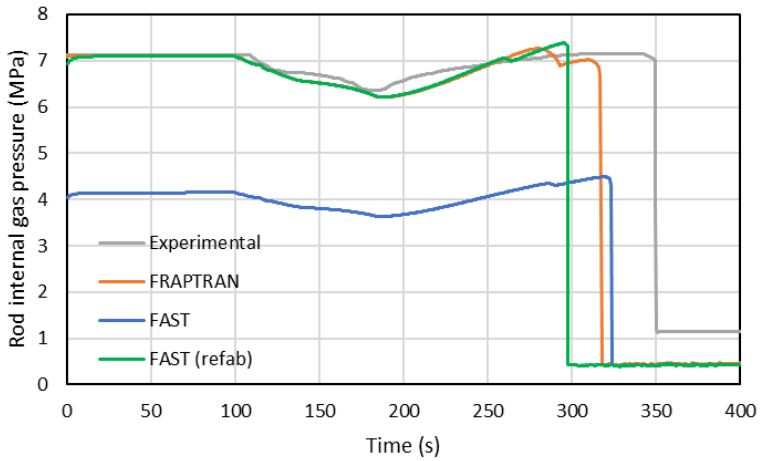

Figure 15. Rod internal gas pressure evolution.

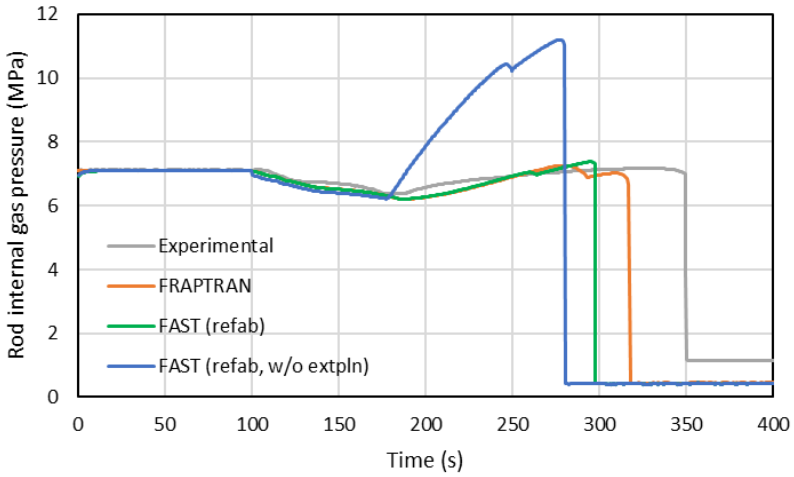

Figure 16. Rod internal gas pressure evolution. Impact of external plenum definition.

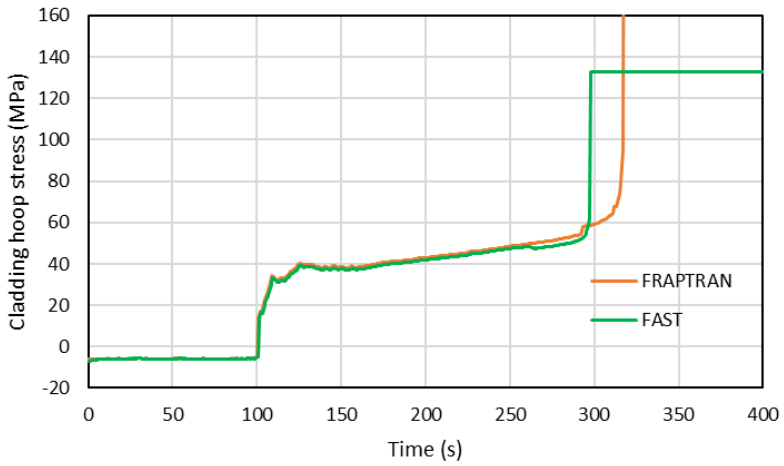

Figure 17. Cladding hoop stress evolution.

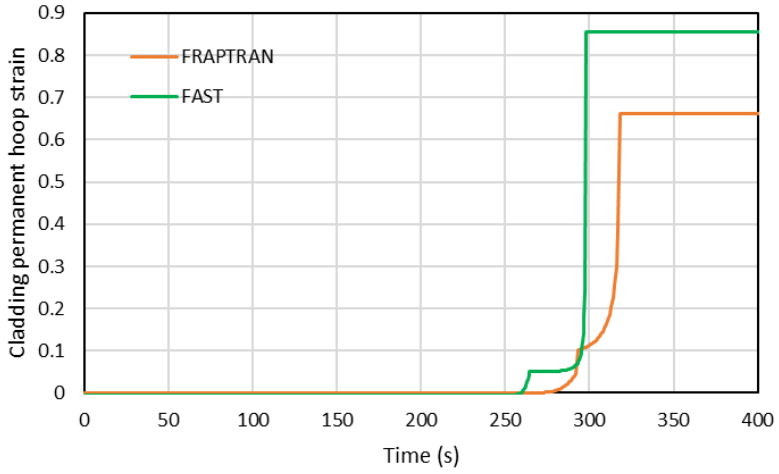

Figure 18. Cladding permanent hoop strain evolution.

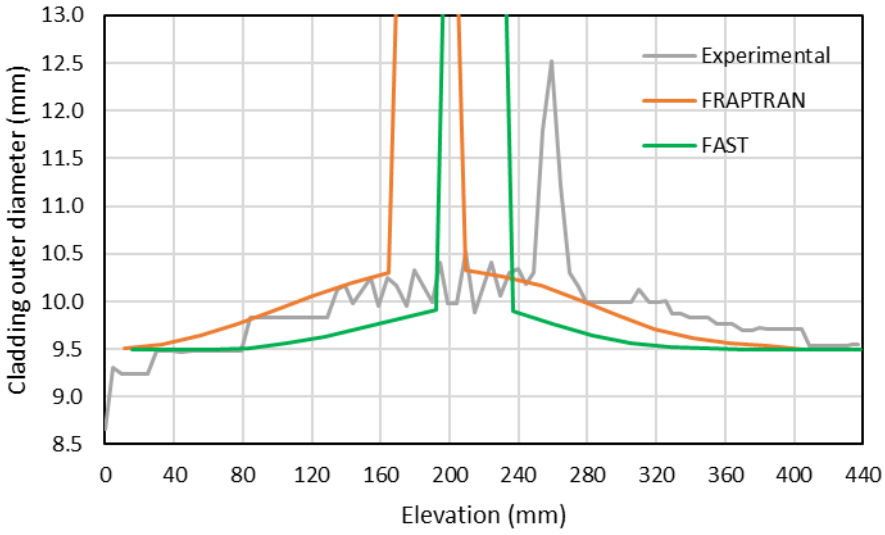

Figure 19. Post-test cladding outer diameter profilometry.

5.2 RIA simulation (FK-1)

Model settings

The average LHR of the D7-5 segment rod during the five irradiation cycles are extracted from the references mentioned in the section 2.2. In the absence of axial power profile data, a flat profile has been assumed for the entire irradiation period. The LHR of the rodlet during the RIA test was extracted from (Sugiyama et al., 2004). Its axial power profile is also considered to be flat. During the base irradiation, the coolant inlet temperature, coolant pressure, and coolant mass flux match the constants shown in Table 3, except for the coolant inlet temperature and pressure at the end of the irradiation, which are set to 25°C and 0.1 MPa, respectively. During the RIA transient, the cladding surface temperature evolution at various elevations and the coolant pressure, assumed to be constant at 0.1 MPa, are specified. As mentioned above, the FK-1 test instrumentation includes three thermocouples attached to the cladding surface at different axial elevations. However, after 1 s into the test, the signal from the top thermocouple (TF3; 85 mm from the bottom of the test rodlet) was lost, so the cladding surface temperature at the corresponding elevation could not be specified. The cladding surface temperatures recorded by the thermocouples at the lower (TF1) and middle (TF2) elevations were input into FAST at their respective axial positions: 21 and 53 mm from the bottom of the test rodlet. The mechanical behavior is modelled using FRACAS-I for small deformations and BALON2 for cladding ballooning (large deformations). Cladding failure is described by both low- and high-temperature models, while FGR is handled with FRAPFGR, and high-temperature oxidation is modelled using the Cathcart-Pawel correlation. The refabrication option is activated at the final time step of the base irradiation simulation, which corresponds to a zero-power cold state (i.e., 0 kW/m, 25 C, and 0.1 MPa). The refabricated plenum length is set to 45.5 mm to match the measured free volume of the test rodlet (3.96 cm^3). The variable axial nodalization option is activated to define the position of the test segment within the mother rod (211-317 mm from the bottom of the segment D7-5) from the start of the base irradiation. In the present simulation, the D7-5 segment is divided into 15 variable-length axial nodes, while the test rodlet nodalization comprises 10 nodes evenly spaced along its active length.

Results and discussion

The target output variables shown in this report are focused on the following ones related to the RIA test calculations: the fuel and cladding outer surface temperatures, cladding hoop stress, cladding permanent hoop strain, cladding failure prediction, and fuel stack and cladding axial elongation. Results are provided at the peak power node (located 58 mm from the bottom of the test rodlet at the beginning of the RIA transient) and as a function of time. Experimental data is available only for the fuel stack and cladding elongation. Data-code comparisons of the post-test cladding outer diameter were not possible, as experimental data are provided only along the axial region above the fuel stack column, where the FAST mechanical model does not perform any calculations. As shown in Figure 20, the maximum temperatures for the fuel and cladding outer surfaces reach 1598 °C and 384 °C, respectively. Both temperatures rise rapidly due to the energy deposited in the pellet by the power pulse, which peaks around 0.205 s, and then decrease as heat is gradually transferred to the coolant. The cladding surface temperature evolution at the peak power node roughly follows the reading from the thermocouple at the middle elevation of the rodlet (TF2). The reasons for the non-smooth trend observed from the end of the power pulse to 1 s into the transient are unclear. At 3.4 s, the fuel-cladding gap begins to open due to the thermal contraction of the pellet, which is cooling down on average. Consequently, the thermal resistance between the pellet and the cladding increases, causing the fuel surface temperature to rise. This trend continues until 7.8 s, when the increase in gap thickness slows, improving heat transfer across the gap and causing the fuel surface to cool once again.

Figure 21 provides a close-up view of the first second of the transient shown in Figure 20, including readings from the lower (TF1) and middle (TF2) thermocouples. At present, it is unclear how the code interpolates the

cladding outer temperature at each elevation of the axial nodalization from the temperature profile specified at each time step in the input file (in this case, at two axial positions).

An additional point for discussion is the validity of comparing experimental measurements from the thermocouples with the predicted cladding surface temperature at a given axial node. For instance, in this simulation, the peak power node is axial node 10, while the TF2 thermocouple is located 53 mm from the bottom of the test rodlet, within the length of node 10. One might expect the values of TCO (plotted at the mid-plane of the PPN) and TF2 to always coincide. However, this is not the case for two reasons. First, the mid-plane elevation of node 10 at the beginning of the transient is 58 mm, slightly deviating from the TF2 position of 53 mm. Second, the position of the axial node mid-plane varies throughout both the base irradiation and the transient due to phenomena such as irradiation axial growth or thermal expansion. This means that the position of the mid-plane is not constant, unlike the position of TF2, where the cladding surface temperature is input into FAST at each time step. Figure 22 illustrates the evolution of the cladding hoop stress. Before the power pulse, the cladding is in a slightly tensile stress state (~1 MPa) due to the external coolant pressure (atmospheric) being lower than the internal gas pressure. During the power pulse, the thermal expansion of the pellet causes hard contact with the cladding, resulting in a non-zero pellet-cladding interfacial pressure. Consequently, the cladding experiences an outward force that triggers an increase in hoop stress, which reaches a maximum of 472 MPa. The cladding yield strength is exceeded during this phase, leading to permanent deformation (see Figure 23). After the power pulse peak, as the pellet cools and undergoes thermal contraction, the cladding hoop stress decreases rapidly until the pellet-cladding interfacial pressure returns to zero (around 0.213 s). At this point, the cladding attains a new stress state determined by the pressure differential across its wall. The cause of the non-physical discontinuity at 0.207 s is unknown, but it is not related to convergence issues within the mechanical calculation. One hypothesis is that this discontinuity may result from the tolerance limits of the convergence algorithm embedded in the closed-gap mechanical calculation. Further investigations with access to the FAST source code would be needed to confirm this hypothesis.

Figure 23 shows the evolution of the cladding permanent hoop strain. The initial negative values, resulting from cladding creep down during the base irradiation, are observed before the power pulse. During the power pulse, as previously mentioned, the cladding yield strength is exceeded, leading to instantaneous (plastic) permanent deformation over two consecutive time steps. After this period, the yield strength is not exceeded for the remainder of the simulation, and the cladding permanent hoop strain remains around 0.7% until the end of the transient.

The cladding failure prediction is defined as $CFP(t) = x(t)/x_{critical}(t)$, where x represents any failure parameter. In the present simulation, $x_{critical}(t)$ is associated with the cladding strain limit. As shown in Figure 24, cladding failure is not predicted for the FK-1 test since the maximum CFP remains below 1, consistent with experimental observations. The low-temperature strain limit in FAST is applied below 700 K and based on previous experience with FRAPTRAN-2.0, only if the cladding permanent hoop strain at a given time step exceeds that of the previous one. Given these constraints, the CFP associated with the low-temperature limit is non-zero only during two consecutive time steps around 0.207 s, resulting in a maximum CFP of 0.37. The high-temperature strain limit is not applied because the average cladding temperature does not reach 940 K throughout the transient.

Figure 25 displays the fuel stack and cladding axial elongation during the transient. A notable observation is the significant overestimation in the FAST prediction for the fuel stack elongation, which is approximately 90% higher than the experimental value during the power pulse. Conversely, the cladding elongation is underestimated, with the largest deviation occurring around 1 s into the transient. However, both predictions align with the experimental data by the end of the test.

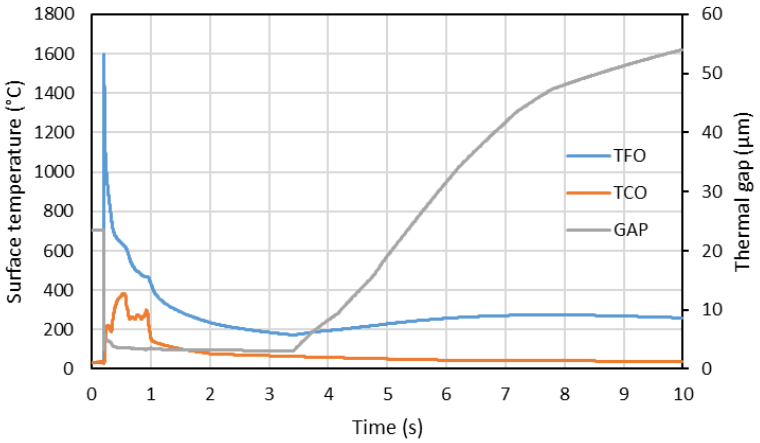

Figure 20. Fuel and cladding surface temperatures and gap width as a function of time.

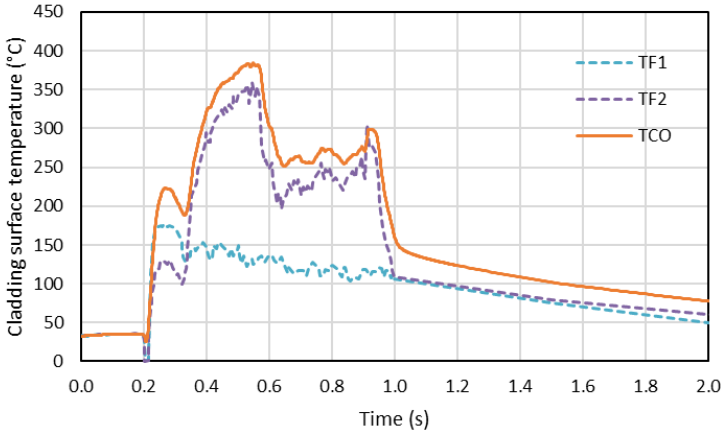

Figure 21. Cladding surface temperature as a function of time.

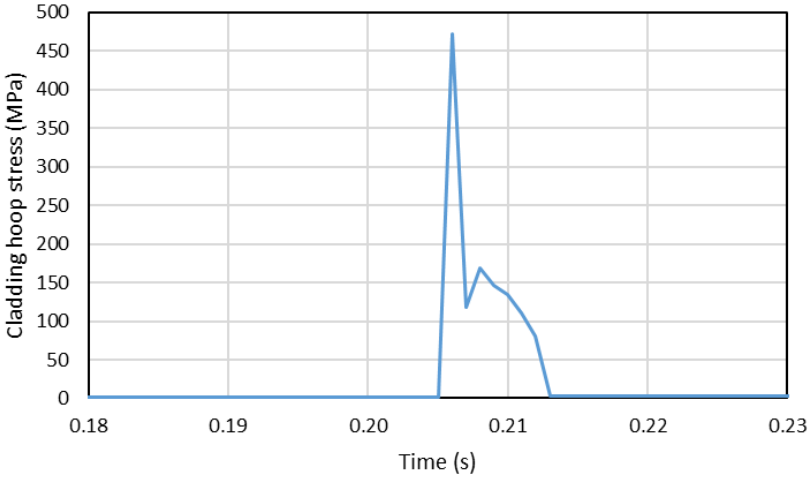

Figure 22. Cladding hoop stress as a function of time.

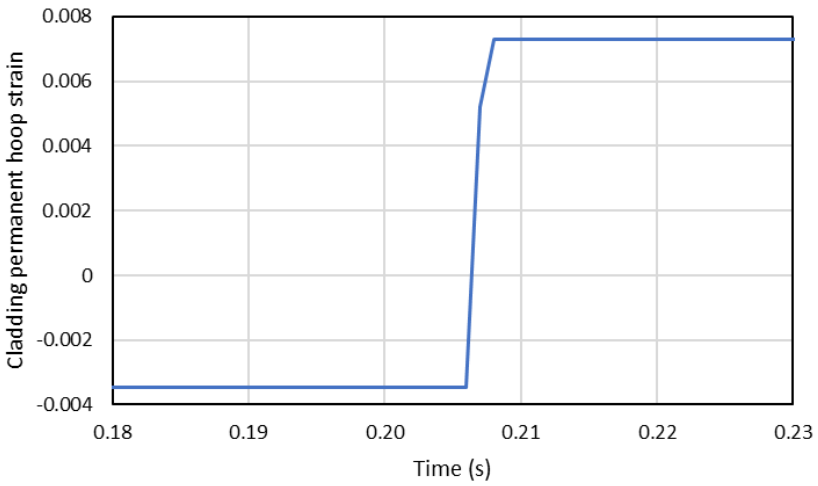

Figure 23. Cladding permanent hoop strain as a function of time.

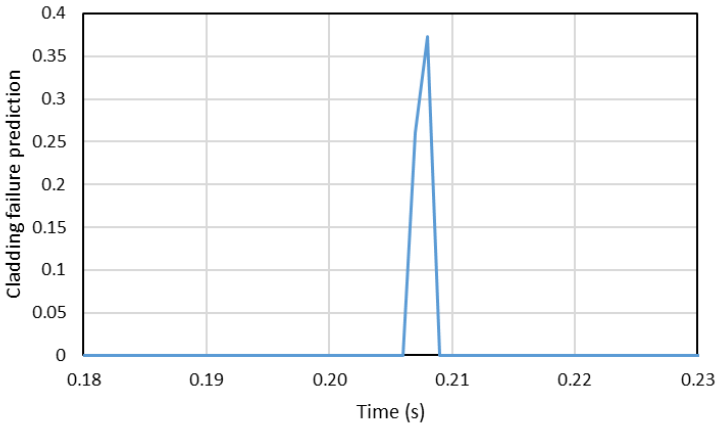

Figure 24. Cladding failure prediction as a function of time.

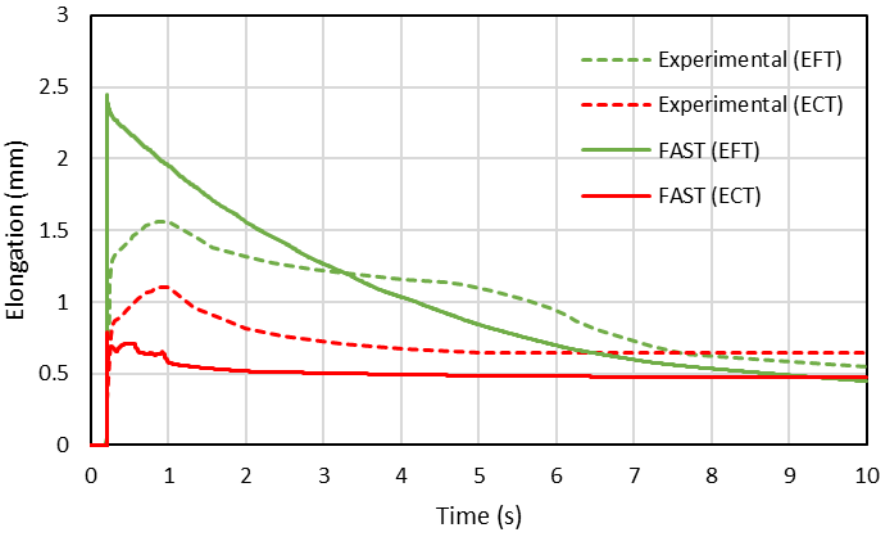

Figure 25. Fuel stack and cladding axial elongation as a function of time.

6 Conclusions

This deliverable presents a comprehensive overview of fuel reference state calculations for selected scenarios, specifically base irradiation, LOCA and RIA conditions, leveraging the expertise of multiple partners and advanced FPCs. The primary objective was to define the fuel reference initial states under transient conditions, supporting the goals of WP3 and serving as a critical input for activities in WP5. Each partner contributed with simulations based on different FPCs:

- PSI applied the FALCON code to simulate both base irradiation (BEAVRS benchmark) and LOCA (MT4) conditions. The simulations provide detailed reference states for multiple physical parameters and will serve as the guidance for validating OFFBEAT simulations in WP5.
- LEI performed RIA simulations with TRANSURANUS, focusing on the FK-1 test. These results characterize key fuel and cladding responses under power pulse conditions.
- POLIMI extended the FK-1 analysis with TRANSURANUS-SCIANTIX, enabling a more detailed physics-based prediction of fission gas release and its impact on pressure, deformation, and gap dynamics.
- CIEMAT used the FAST code to simulate LOCA and RIA scenarios (IFA-650.10 and FK-1), applying advanced mechanical and high-temperature models to capture key transient behaviors.

A harmonized case description and a shared data comparison template (provided by CIEMAT) ensured coherence and traceability across different simulation tools. These coordinated efforts strengthen the robustness of the fuel modeling framework within OperaHPC.

References

Bohn, M. P. (1977). *FRACAS: a subcode for the analysis of fuel pellet-cladding mechanical interaction*. https://doi.org/10.2172/7219131

Bykov, V., Vasiliev, A., Ferroukhi, H., & Pautz, A. (2016, March). *Solution of the Beavrs Benchmark using CASMO-5 / SIMULATE-5 Code Sequence*.

Geelhood, K. J., Beyer, C. E., & Luscher, W. G. (2008). *PNNL Stress/Strain Correlation for Zircaloy Prepared for the US Nuclear Regulatory Commission Division of Spent Fuel Storage and Transportation*. http://www.ntis.gov/ordering.htm

Geelhood, K. J., Colameco, D. V., Luscher, W. G., Kyriazidis, L., Goodson, C. E., Corson, J., & Whitman, J. J. (2022). *FAST-1.1: A Computer Code for Thermal-Mechanical Nuclear Fuel Analysis under Steady-state and Transients (Developed under NQA-1-2017)*. https://doi.org/10.2172/2331463

Hagrman, D. L. (1981). *EGG-CDAP-5379, Fuel Behavior Model Development, Zircaloy Cladding Shape at Failure (BALON2).*

Hagrman, D. L., & Reymann, G. A. (1979). *MATPRO-Version 11: a handbook of materials properties for use in the analysis of light water reactor fuel rod behavior*. https://doi.org/10.2172/6442256

Hagrman, D. T., Allison, C. M., Berna, G. A., others, and, & Nuclear Regulatory Commission Washington, D. C. (United S. Div. of S. T. (1995). *SCDAP/RELAP5/MOD 3.1 code manual: MATPRO, A library of materials properties for Light-Water- Reactor accident analysis. Volume 4*.

Horelik, N., Herman, B., Ellis, M., Kumar, S., Liang, J., Forget, B., & Smith, K. (2018). *Benchmark for Evaluation And Validation of Reactor Simulations RELEASE rev. 2.0.2*.

Jernkvist, L. (2005). *Evaluation of the RIA simulation tests FK-1, FK-2 and FK-3 on high-burnup BWR fuel rods*.

Khvostov, G., Wiesenack, W., B.C.Oberländer, Kolstad, E., Ledergerber, G., & Zimmermann, M. (2011, March). *Post-test analysis of the Halden LOCA experiment IFA-650.7 using the FALCON code*.

Lassmann, K., O'Carroll, C., van de Laar, J., & Walker, C. T. (1994). The radial distribution of plutonium in high burnup UO2 fuels. *Journal of Nuclear Materials*, *208*(3), 223–231. https://doi.org/10.1016/0022-3115(94)90331-X

Lavoil, A. (2010). LOCA Testing at Halden; The Tenth Experiment IFA-650.10. *HWR-974, OECD Halden Reactor Project*.

Limbäck, M., & Andersson, T. (1996). A Model for Analysis of the Effect of Final Annealing on the In- and Out-of-Reactor Creep Behavior of Zircaloy Cladding. *ASTM Special Technical Publication*, *1295*, 448–468. https://doi.org/10.1520/STP16185S

Nishi, N., & Lee, B. H. (2001). *Summary of pre-irradiation data on fuel segments supplied by EDF/FRAMATOME and tested in IFA-610, 629 and 648. HWR-664*. OECD Halden reactor project.

Rashid, Y., Dunham, R., & Montgomery, R. (2004). Fuel analysis and licensing code: FALCON MOD01. *EPRI Report*, *1011308*, 1315–1755.

Sugiyama, T., Nakamura, T., Kusagaya, K., Sasajima, H., Nagase, F., & Fuketa, T. (2004). *Behavior of irradiated BWR fuel under reactivity-initiated-accident conditions, Results of tests FK-1, -2 and -3* (Issue JAERI-Research 2003-033).

Wilson, C. L., Mohr, C. L., Hesson, G. M., Wildung, N. J., Russcher, G. E., Webb, B. J., & Freshley, M. D. (1983). LOCA Simulation in NRU Program: Data Report for the Fourth Materials Experiment (MT-4). In *NUREG/CR-3272 (PNL-4669)*. Pacific Northwest Laboratory.